Combined effect of grain shape and grading on the small-strain stiffness of granular soils at different densities and stress states

Qian Gu, M. Sc., Debdeep Sarkar, M. Sc.
Dr.-Ing. Meisam Goudarzy and Prof. Dr.-Ing. habil. Torsten Wichtmann
Ruhr-Universität Bochum

This research presents an experimental study on the combined effect of particle shape and grain size distribution on the small-strain stiffness of granular materials. Three materials with significantly different grain shapes - angular crushed glass, sub-angular Rhein sand, and round glass beads were tested with two different grain size distribution curves. Air-pluviated triaxial samples with different densities were tested at isotropic and anisotropic stress states. The shear and compression wave velocities across different directions were determined using piezoelectric elements. Based on the experimental data the combined influence of grain shape and grading on the small-strain stiffness moduli G_{max} and E_{max} as well as Poisson's ratio ν is analyzed. The stiffness anisotropy is judged based on G_{max} values measured in different directions and with different polarization. The parameters of empirical equations for G_{max} and E_{max} are inspected with respect to the influence of grain shape.

1 Introduction

Soil stiffness is of primary importance in a number of geotechnical problems including foundation settlement, deformations caused by excavations or wave propagation in the ground due to vibration. The dependence of the stiffness on strain level is well known. This paper concentrates on the maximum stiffness at very small strain levels ($\gamma < 10^{-6}$). In the laboratory this maximum stiffness can be determined, amongst others, from wave velocity measurements with piezoelectric elements. The compression and shear wave velocities, v_P and v_S, are measured using compression and bender elements respectively. The small-strain constrained (oedometer) and shear modulus, M_{max} and G_{max}, are calculated from these velocities using Equation 1:

$$M_{max} = \rho v_p^2 \quad ; \quad G_{max} = \rho v_s^2 \qquad (1)$$

where ρ denotes mass density. The small-strain Young's modulus E_{max} and Poisson's ratio ν are obtained from M_{max} and G_{max} using the formulas of classical elasticity.

Since the 1960s, the dependency of G_{max} on various parameters, in particular void ratio and effective stress has been examined, mainly on specimens subjected to isotropic stresses. The majority of measurements were made along the vertical direction using waves with a horizontal polarization. The G_{max} value determined in such experiments is also denoted as G_{vh}, where the first index denotes the direction of wave propagation while the second one denotes the direction of polarization. Hardin and Black (1966) proposed one of the most widely used empirical equations for G_{vh}:

$$G_{vh} = A\, p_a\, f(e)\, (p'/p_a)^n \qquad (2)$$

with atmospheric pressure pa = 100 kPa and the fitting parameters A and n. Two void ratio functions proposed by either Hardin and Black (1966) or Jamiolkowski et al. (1995) are popular:

$$f(e) = (c-e)^2/(1+e) \quad ; \quad f(e) = e^{-d} \qquad (3)$$

with fitting parameters c and d. Since A, n, c and d are material constants they depend on the grain size distribution and grain shape (e.g. Wichtmann and Triantafyllidis 2009 and Payan et al. 2016).

An anisotropy of the stiffness can result from the specimen fabric which is affected by various parameters, e.g. sample preparation, particle characteristics and stress states. The inherent and stress-induced anisotropy can be detected from variations in the magnitudes of the wave velocities measured in different directions (Pennington et al. 1997; Kuwano and Jardine 2002; Gasparre et al. 2007). A brief literature review is given in the following.

1.1 Inherent anisotropy in soils

To judge anisotropy, beside G_{vh} and the Young's modulus E_v in the vertical direction, the stiffnesses along other directions and with different polarization, e.g. E_h, G_{hh} and G_{hv} along the horizontal direction must be determined, for example using compression or bender elements mounted on the lateral boundary of a triaxial sample.

Jamiolkowski et al. (1995) tested the small-strain stiffness of six clays in oedometer and resonant column tests with isotropic stress conditions using bender elements mounted at the sides and found a higher G_{hh} compared to G_{vh}. Likewise, Bellotti et al. (1996) reported the ratio of G_{hh}/G_{hv} to lie between 1.14 and 1.21 under isotropic stress conditions, based on wave velocity measurements performed in a calibration chamber equipped with geophones. Also Kuwano and Jardine (2002) showed that the ratio of G_{hh} to G_{hv} for saturated Ham river sand consolidated isotropically was larger than 1. Using hollow cylinder and triaxial tests on Toyoura sand with isotropic stress conditions, Chaudhary et al. (2004) found that both the Poisson's ratio as well as the Young's modulus in the horizontal direction were higher than the corresponding values in the vertical direction. Similar observations denoting a higher G_{hh} compared to G_{hv} for isotropically consolidated undisturbed and reconstituted samples of various sands were reported by Yamashita et al. (2005), who used bender elements installed in a triaxial device. Sadek et al. (2007) conducted a series of bender element tests on Hostun sand applying a modified true triaxial device. Their results confirmed that G_{hh} was larger than G_{vh}, while the difference was influenced by the direction along which the sand was filled into the true triaxial box. The same tendency was also reported by Wang and Mok (2008) from experiments on Toyoura sand using a true triaxial device. The differences in the measured stiffness moduli or Poisson's ratios for different directions are due to the inherent anisotropy of the fabric of the material, which mainly results from specimen preparation.

1.2 Influence of mean grain size and gradation

Several studies demonstrate the significant effect of the particle characteristics of granular materials, in particular grain size distribution and particle shape on elastic stiffness. The available studies were restricted to G_{vh} and E_v, however.

The influence of mean grain size D_{50} is still debatable. Some studies (e.g. Iwasaki and Tatsuoka 1977; Wichtmann and Triantafyllidis 2009; Yang and Gu 2013) suggest that D_{50} doesn't influence the small-strain stiffness of granular materials while others (e.g. Menq and Stokoe 2003; Hardin and Kalinski 2005) found an increase in stiffness with increasing mean grain size. Furthermore, most authors (e.g. Iwasaki and Tatsuoka 1977; Wichtmann and Triantafyllidis 2009; Payan et al. 2016) have reported that the small-strain shear stiffness decreases with increasing uniformity coefficient C_u at constant void ratio. However, Menq and Stokoe (2003) found the opposite trend when considering similar relative density, with slightly higher G_{max} values for dense specimens with $C_u = 10$ compared to $C_u = 1.2$.

1.3 Influence of grain shape

Experiments have been also conducted to investigate the effect of particle shape on the small-strain stiffness of granular soils. In studies by Lo Presti et al. (1997), Bui (2009), Senetakis et al. (2012) and Payan et al. (2016), at a given void ratio and confining pressure, the measured small-strain shear moduli of rounded sands were generally higher than in their sub-angular or angular counterparts. Hardin and Richart (1963) reported that the material constant c of the void ratio function defined by Eq. 3 is significantly affected by particle shape, with a higher c value for rounded materials. The relation between the pressure exponent n and grain shape is discussed controversially. Some studies found a decreasing trend of n with increasing roundness (Cho et al. 2006; Payan et al. 2016) while some others encountered the opposite (Liu and Yang 2018; Goudarzy and Wichtmann 2019). Altuhafi et al. (2016) observed that n varies randomly.

1.4 Stress-induced anisotropy

Numerous studies have been done to assess the effects of stress-induced anisotropy on small-strain stiffness of soils (Kuribayashi et al. 1975; Roesler 1979; Yu & Richart 1984; Santamarina and Cascante 1996; Wang and Mok 2008; Sadek et al. 2007; Goudarzy et al. 2018). All these studies revealed that the small-strain shear stiffness G_{vh} is affected by the vertical and horizontal stresses acting in the directions of shear wave propagation and polarization, respectively.

Roesler (1979) performed wave velocity measurements in cuboidal sand samples under different stress states. He proposed an empirical relation to predict the shear wave velocity for anisotropic stress conditions considering the influence of the three stress components σ_a, σ_p and σ_s acting in the directions of shear wave propagation, wave polarization and orthogonal to that plane. Based on Roesler's approach and analogous to Eq. (2) the small-strain shear modulus G_{vh} can be formulated as:

$$G_{vh} = A\, f(e)\, (\sigma'_v/p_a)^{n_v}\, (\sigma'_h/p_a)^{n_h}\, (\sigma'_s/p_a)^{n_s} \qquad (4)$$

with $\sigma_a = \sigma'_v$, $\sigma_p = \sigma'_h$ and the fitting parameters n_v, n_h and n_s. Experimental observations show that the wave velocities are not influenced by the stress acting normal to the plane containing the directions of wave propagation and polarization (e.g. Sadek et al. 2007), i.e. $n_s = 0$ can be assumed. Equation 4 has been widely used to describe the effect of anisotropic stress states on small-strain stiffness (e.g. Yu and Richart 1984, Belotti et al. 1996; Zeng and Ni 1998; Fioravante 2000; Sadek et al. 2007; Hardin and Black 1966; Yu and Richart 1984; Santamarina and Cascante 1996; Goudarzy et al. 2018).

Few studies have also attempted to determine the effect of stress anisotropy on the shear stiffness in different directions, i.e. G_{vh}, G_{hh} and G_{hv}, using bender elements (e.g. Belotti et al. 1996; Fioravante 2000; Chaudhary et al. 2004; Shi et al. 2021). Jardine et al. (1999) showed that under anisotropic stress conditions in triaxial tests G_{vh} is larger than G_{hh} for both Ham river sand and glass ballotini. In their experiments G_{vh} differed from G_{hv}, which was argued as an effect of the measurement method. They proposed to adopt an average value of G_{vh} and G_{hv} in the stiffness matrix. From hollow cylinder and triaxial tests on Toyoura sand, Chaudhary et al. (2004) found that the difference between the vertical and horizontal Young's moduli ($E_h > E_v$) decreased with increasing stress anisotropy till $K = \sigma'_h/\sigma'_v = 0.5$ where $E_h = E_v$ was measured. At higher anisotropic stress states, Sadek et al. (2007) found both the shear and compression wave velocities in Hostun sand to be larger in the vertical direction than in the horizontal direction, opposite to isotropic stress conditions. Similar results on calcareous sands were recently reported by Shi et al. (2021) from triaxial tests with bender elements.

1.5 Motivation of current research

Previous studies have mainly focused on the influence of various particle characteristics (such as D_{50}, C_u or shape) on the moduli G_{vh} and E_v. To the best knowledge of the authors, there is no study investigating the effect of particle gradation and shape on the other parameters of the cross-anisotropic elastic stiffness (beside G_{vh}: G_{hv}, G_{hh}, E_v, E_h and Poisson's ratio along various directions ν_{vh}, ν_{hv} and ν_{hh}). In the current study, a respective investigation is undertaken in a series of tests on two different gradations in combination with three different grain shapes. A triaxial device with end plates equipped with compression and bender elements was used, along with additional bender elements mounted at the lateral boundary of the sample. In that way G_{vh}, G_{hv}, G_{hh}, E_v and ν_{vh} (denoted ν herein) could be measured.

2 Experimental program

2.1 Test device

The triaxial device used allows measurements of wave velocities not only in the vertical but also along the horizontal directions of the specimen. A photo of the system without the pressure cell is shown in Fig. 1a. The top and bottom caps were equipped with a pair of compression and a pair of bender elements to measure compression and shear wave velocities in the vertical direction, $v_{P,v}$ and $v_{S,vh}$ (Fig. 1g). Shear waves in the horizontal direction were measured with two pairs of bender elements mounted on the side of the specimens. These horizontal bender elements consist of two parts: i) a PVC socket, which penetrates into the membrane of the sample to orient the bender element and connect it to the sample (Fig. 1b) and ii) a removable PVC plug which carries the bender elements (Fig. 1c). With a horizontal orientation of the bender element one measures $v_{S,hv}$ (vertical polarization), with a vertical one $v_{S,hh}$ (horizontal polarization).

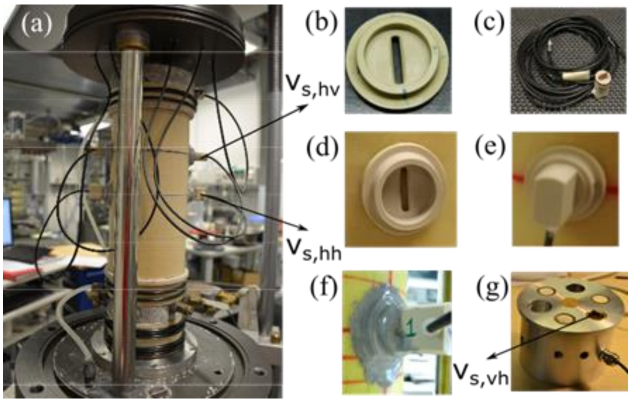

Fig. 1: (a) Triaxial device employed in the present study, equipped with piezoelectric elements for wave velocity measurements in b-f) horizontal direction (mounted on sides of sample) and g) vertical direction (integrated in end plates)

The experiments were conducted on samples measuring 20 cm in height and 10 cm in diameter. Membranes of thickness 0.7 mm were used throughout. The vertical loading was applied with an electromechanical load press. Vertical deformation was measured using a LVDT mounted to the load piston. The volume change of the sample was determined based on the expelled pore water using a burette system and a differential pressure transducer. The cell and back pressures were also measured using two sensors.

The piezoelectric elements were connected with cables to a measuring system that comprises of two amplifiers, a data logger and a computer with LabVIEW software (Fig. 2). For initial calibration of the system, rods made out of aluminum and plastic were used. The delay time ($\Delta t = 0.00002$ s) in the measurement system was determined bringing the transmitting and receiving elements in direct contact. The delay time was subtracted from the traveling time measured in the soil samples. A sinusoidal waveform, which was also previously used by Yamashita et al. (2009), Azeiteiro et al. (2017) and Shi et al. (2021), was applied as the transmitted signal. The travelling time was measured using the first deflection method adopted in previous studies by Yamashita et al. (2009), Goudarzy et al. (2016) and Gu et al. (2020).

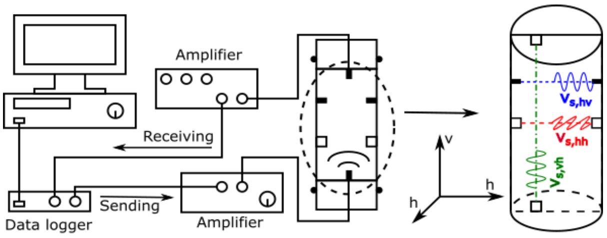

Fig. 2. Schematic representation of the bender elements and devices employed to measure shear waves in various directions. Compression elements were only mounted in the end plates, measuring in vertical direction.

2.2 Materials tested

In the experiments, three granular materials having visibly differing grain shapes are used: angular crushed glass, sub-angular Rhein (Rhine) sand and round glass beads. The glass beads were obtained from a local supplier (Mühlmeier GmbH). The crushed glass was produced by mechanically crushing round glass beads using a Los Angeles abrasion machine, and then separating the fines by thoroughly washing over a 0.063 mm sieve. After sieving, for each of the three materials two mixtures with identical mean grain size D_{50} = 0.45 mm but different uniformity coefficient C_u = 1.25 or 5 respectively were prepared (see Fig. 3). The grain size distribution, specific gravity and the maximum and minimum void ratios (see Table 1) were determined in accordance with DIN 18123, 18124 and 18126. The grain shape parameters were obtained through analysis of images taken with a digital microscope, further details of which may be found in Sarkar et al. (2019). The current study utilizes three shape parameters: 2D roundness (R), 2D sphericity (S) and regularity (ρ) which is the mean of R and S. Roundness, a medium/meso scale descriptor, is defined as the ratio of the average radius of curvature of the corners of a particle to the radius of the maximum inscribed circle. Although various definitions of the macro scale descriptor sphericity exist, the most common one is considered herein, where S is calculated as the ratio of the diameter of the largest circle that can be inscribed into the particle to the diameter of the smallest circle that circumscribes the particle. As either roundness or sphericity alone is not sufficient to describe grain shape adequately, the regularity factor ρ was suggested by Cho et al. (2006) to capture both features in one parameter.

2.3 Sample preparation and testing

For each material samples with different relative densities were prepared by air pluviation. A vacuum of 50 kPa was applied through the drainage lines to stabilize the specimen during installation of the horizontal bender elements. To install the horizontal bender elements, the socket part was glued to the membrane. It contains a rectangular slot (Fig. 1d) which allows the membrane to be cut using a sharp blade. The plug was then pushed into the socket (Fig. 1e), leading to a penetration of the bender element into the soil sample. An O-ring seal makes the plug and socket connection water-tight. After assembly of the elements the whole system was coated with glue to fix the elements in their place and to guarantee sealing (Fig. 1f). The glue was left to dry for a minimum of 2 hours, after which the sealing was checked. The bender transducer was held firmly in place during tests by the cell pressure. Once the integrity of the membrane with the elements was ensured, the tests were carried forward and the triaxial cell was assembled. To achieve a good saturation, carbon dioxide was flushed through the sample followed by saturation with deionized and de-aired water. A back pressure of 200 kPa was used to dissolve remaining air bubbles. B-values greater than 0.95 were achieved in all tests.

Table 1. Physical properties of the six materials

Material	C_u [-]	ρ [-]	e_{max} [-]	e_{min} [-]	G_s [-]
Crushed glass	1.25 5	0.45	1.15 1.03	0.68 0.50	2.54
Rhein sand	1.25 5	0.60	0.90 0.83	0.57 0.47	2.65
Round glass	1.25 5	0.90	0.74 0.53	0.58 0.38	2.54

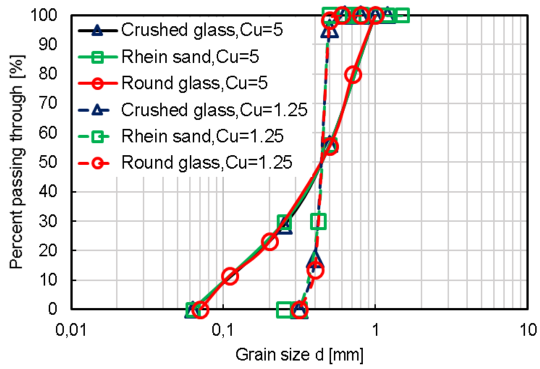

Fig. 3: Grain size distribution of the tested materials.

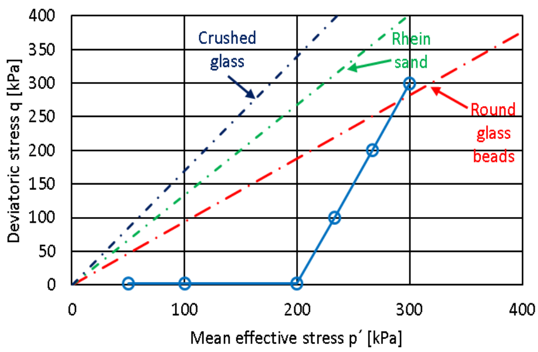

Fig. 4: Effective stress paths applied in the tests; the blue, green and red dashed lines represent the failure lines obtained from drained monotonic triaxial tests on loose samples (Sarkar et al. 2019)

The effective stress path applied in all tests is shown in Fig. 4. Initially an isotropic stress path was followed. In that phase the mean effective stress was increased from p' = 50 kPa over 100 kPa to 200 kPa. Afterwards a phase with anisotropic stresses followed, where the effective lateral stress was kept constant at σ_h' = 200 kPa, while the axial effective stress was further increased to σ_v' = 300, 400 and 500 kPa, resulting in deviatoric stresses of q = 100, 200 and 300 kPa. The majority of the tests was performed on the well-graded materials with C_u = 5 while to assess the influence of gradation, a few tests were also done on the uniformly graded materials with C_u = 1.25.

3 Test results

3.1 Influence of stress state, void ratio and grain shape on G_{max}

The influence of the isotropic or anisotropic stress state on the small-strain stiffness G_{max} measured along different directions and with different polarization of the shear waves (G_{vh}, G_{hv}, G_{hh}) is shown for dense specimens (D_r = 0.90) of the well-graded materials in Fig. 5.

For all the test materials, under isotropic stress conditions (σ_v' ≤ 200 kPa), the three different stiffnesses increase with increasing axial stress or mean effective stress p', respectively. The differences in the stiffnesses G_{vh}, G_{hv} and G_{hh} are relatively small. The impact of grain shape on G_{max} at similar relative densities can also be judged from Fig. 5. The small-strain stiffness along the isotropic path is least for the angular crushed glass, while being larger for the round glass beads and the subangular Rhein sand, which show quite similar values.

During anisotropic loading (σ'_v > 200 kPa), G_{vh} and G_{hv} further increase with increasing axial stress. Thereby, G_{hv} grows at a smaller rate than G_{vh}. In contrast, G_{hh} even slightly reduces during the anisotropic loading phase. This decrease is most pronounced for the round glass beads and relatively independent of density. Furthermore, as evident from Fig. 5, for anisotropic stress conditions, the G_{hv} and G_{vh} values of the materials increase with increasing roundness and sphericity of the particles. As expected a decrease in void ratio e results in an increase of G_{vh}, G_{hv} and G_{hh} (Fig. 6).

The test results may be explained through a micromechanical interpretation: At isotropic states the soil fabric is almost isotropic. However, increasing the vertical loading while keeping the horizontal one constant results in an increase of normal contact forces between grains in the vertical direction, while the horizontal ones remain almost the same. This causes a higher shear wave velocity $v_{S,vh}$ and thus stiffness G_{vh} in the vertical direction (see Goudarzy et al. 2018 for further micromechanical argumentations on the impact of the stress anisotropy). Considering the horizontal directions, the vertically polarized signals ($v_{S,hv}$, G_{hv}) benefit by the application of vertical load as well. For the horizontally polarized waves, $v_{s,hh}$, the additional vertical loading results in destabilization of the contacts in horizontal direction. Due to buckling of force chains under higher vertical stress, the number of horizontal contacts decreases and the fabric is weakened leading to lower stiffness in the horizontal direction, especially in case of $v_{s,hh}$ (Goudarzy 2015).

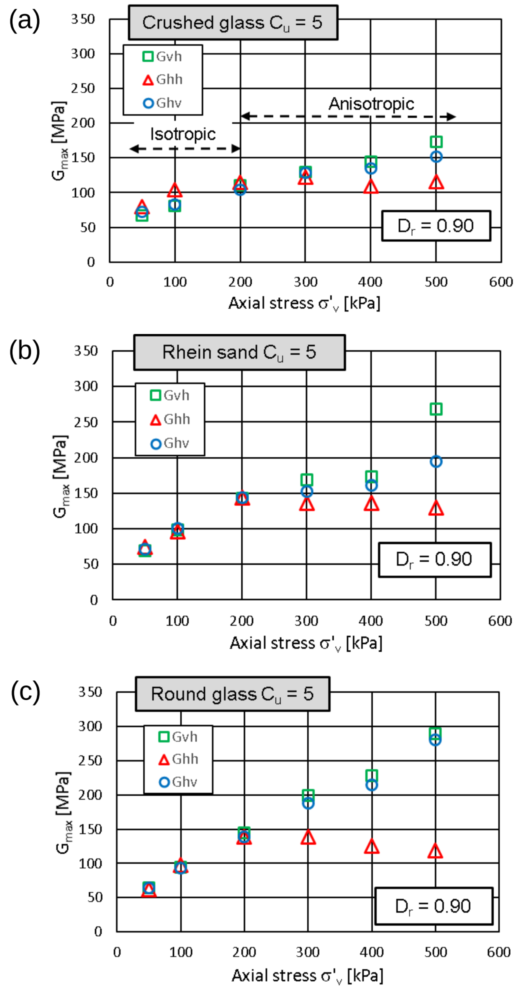

Fig. 5. Variation of small-strain shear stiffnesses G_{vh}, G_{hh} and G_{hv} with axial effective stress under both isotropic and anisotropic stress states

3.2 Influence of stress state, void ratio and grain shape on E_{max}

Young's modulus was measured only along the vertical direction, i.e. E_{max} = E_v. In Fig. 7 results are shown for the well-graded angular crushed glass. Fig. 7a presents the variation of E_{max} with axial stress at different void ratio. It is clear that E_{max} increases with increasing σ_v' and decreasing e for both isotropic and anisotropic stress states. The dependence of E_{max} on e is also visible in Fig. 7b.

The influence of grain shape on E_{max} was observed to be quite similar to that on G_{max} reported in the previous section.

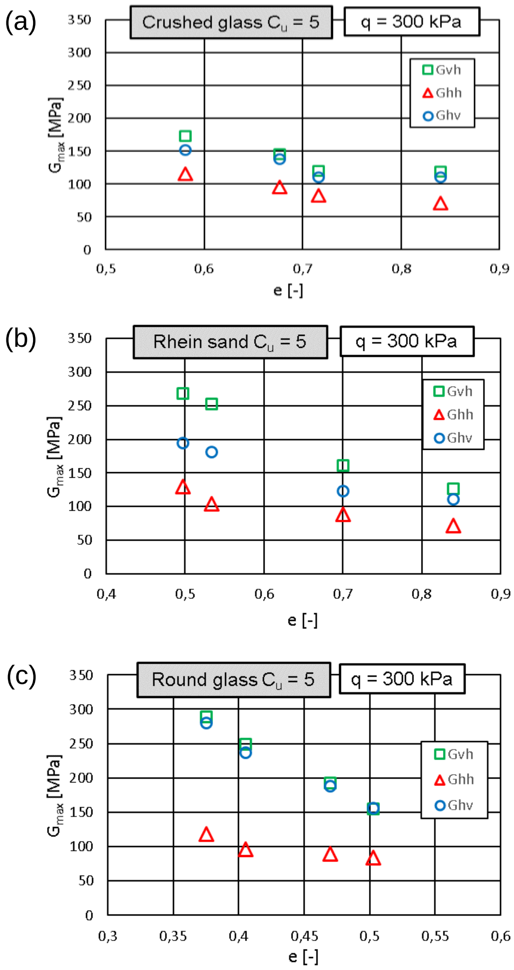

Fig. 6. Variation of the shear stiffnesses G_{vh}, G_{hh} and G_{hv} with void ratio under an anisotropic stress state with q = 300 kPa

3.3 Influence of stress state, void ratio and grain shape on Poisson's ratio

Poisson's ratio ν was determined for the vertical direction only, based on the G_{vh} and E_v data. Values for the well-graded materials are provided in Fig. 8. From Fig. 8a, it is clear that ν reduces slightly with e. The influences of axial stress (Fig. 8b) and grain shape seem negligible. An average value of $\nu \approx 0.3$ was observed in this study.

3.4 Influence of particle size distribution on G_{max} and E_{max}

To assess the influence of the uniformity coefficient C_u on the dynamic stiffnesses of granular soils, the G_{vh}, G_{hv} and G_{hh} as well as the E_{max} values for all six materials were compared at a similar D_r of 0.45. As a representative result, the data for the two gradations of Rhein sand are shown in Fig. 9.

The values of G_{vh} and G_{hh} for the uniformly graded sand (C_u = 1.25) are larger than for the well-graded material (C_u = 5), Fig. 9a. This difference is observed to be relatively small under isotropic stress conditions. With increasing anisotropy of stress, however, the difference in the G_{vh} values increases while it remains almost constant for G_{hh}. While the E_{max} values for both gradations are quite similar under isotropic stress conditions, they increase faster with increasing stress anisotropy for C_u = 1.25 than for C_u = 5 (Fig. 9b).

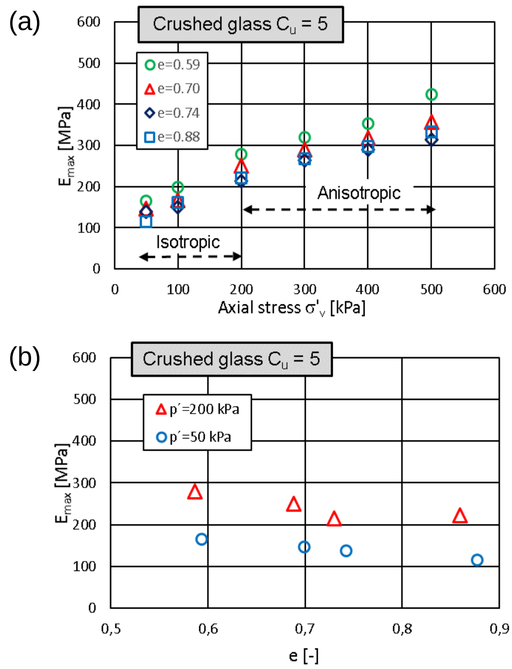

Fig. 7. Variation of E_{max} with a) vertical stress σ_v' and b) void ratio e for angular crushed glass (C_u=5)

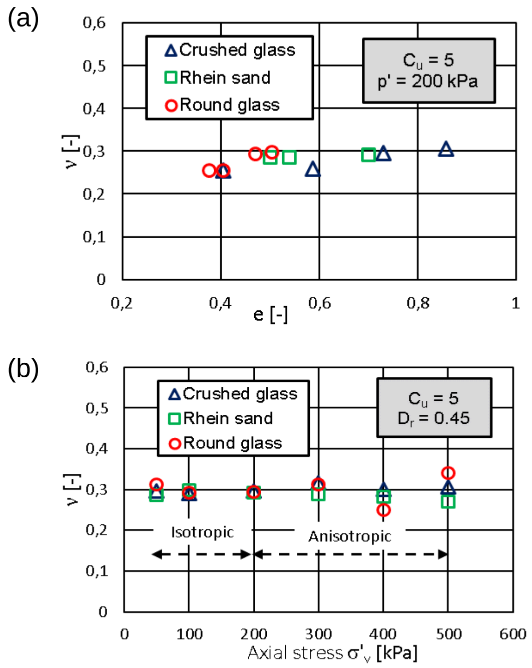

Fig. 8. Variation of Poisson's ratio ν against (a) void ratio for p' = 200 kPa, and (b) axial stress σ_v' for D_r = 0.45 for the well-graded materials

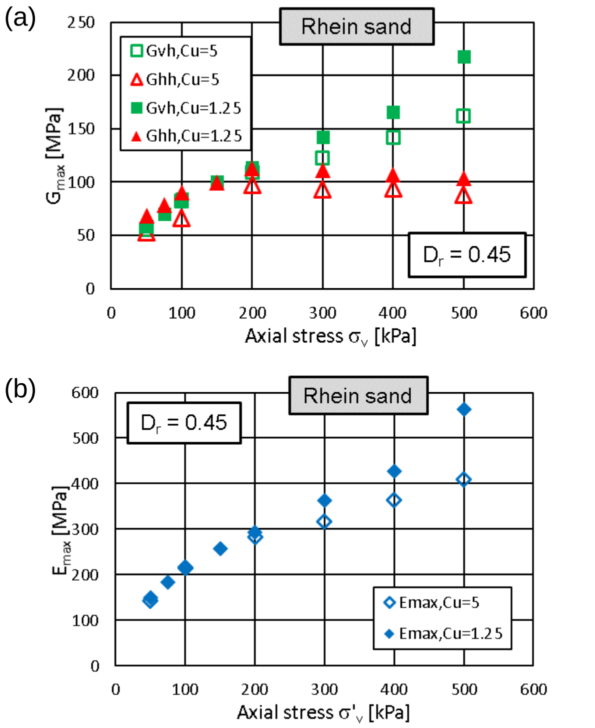

Fig. 9. Variation of (a) G_{vh} and G_{hh}, and (b) E_{max} with axial stress for two different gradations of Rhein sand

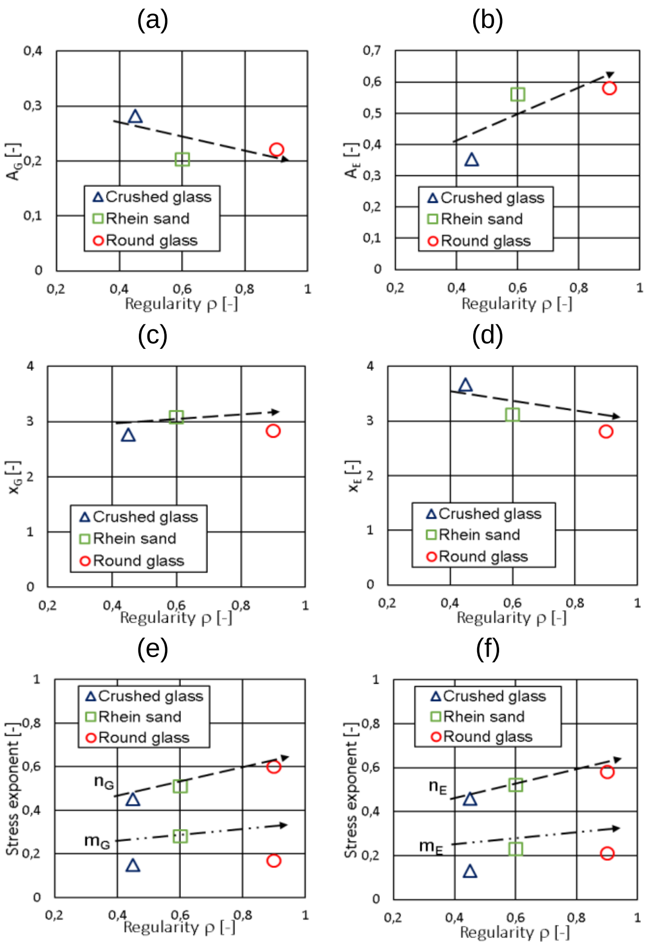

Fig. 10: Fitting parameters of Eqs. (5a) and (5b) for G_{max} and E_{max} plotted against regularity

4 Empirical equations

To predict the stiffnesses $G_{max} = G_{vh}$ and $E_{max} = E_v$ for anisotropic stress states, Equation 2 was extended in the following way:

$$G_{max}=A_G\, p_a\, (x_G-e)^2/(1+e)\, (p'/p_a)^{n_G}\, (1+q/100)^{m_G} \quad (5a)$$
$$E_{max}=A_E\, p_a\, (x_E-e)^2/(1+e)\, (p'/p_a)^{n_E}\, (1+q/100)^{m_E} \quad (5b)$$

Poisson's ratio can be obtained from $\nu=E_{max}/(2G_{max})-1$. The dependence of the fitting parameters of Eqs. (5) on grain shape, described by regularity, is analysed in Fig. 10. The data refers to the well-graded materials with $C_u = 5$. A decrease of A_G and an increase of A_E with increasing regularity ρ is evident in Figs. 10a and 10b. The fitting parameter x_G of the void ratio function slightly increases with ρ (Fig. 10c) while x_E slightly decreases (Fig. 10d). Both the exponents n_G and n_E for the influence of isotropic stress and the stress anisotropy exponents m_G and m_E show a tendency to increase with ρ, which is, however, less pronounced for the m values (Figs. 10e and 10f).

5 Summary and conclusions

The influence of grain shape, gradation and stress anisotropy on the small-strain stiffness of granular materials was investigated. Glass beads, natural sand and crushed sand were tested with two different gradations. A triaxial device equipped with bender and compression elements was applied to measure wave velocities in different directions and with different polarization. Under isotropic stress conditions stiffnesses G_{vh}, G_{hv} and G_{hh} almost coincide and increase with increasing mean effective stress p' and decreasing void ratio e. Under anisotropic stress conditions these stiffness values become different. The magnitude of G_{hh} is the least while G_{vh} is the largest; G_{hv} lies in between. Furthermore, at similar relative density and anisotropic stress states, the E_{max} and G_{max} values are generally larger for uniformly graded materials compared to well-graded ones, while the influence of gradation is less pronounced at isotropic stresses. Poisson's ratio was found to be relatively independent of grain shape and stress anisotropy, with an average value of around 0.3. Finally, the influence of grain shape on the parameters of extended empirical equations for $G_{max} = G_{vh}$ and $E_{max} = E_v$ was quantified.

References

Altuhafi, F. N., Coop, M. R. and Georgiannou, V. N. (2016). Effect of Particle Shape on the Mechanical Behavior of Natural Sands, Journal of Geotechnical and Geoenvironmental Engineering, 142(12): 04016071.

Azeiteiro, R. J. N., Coelho, P. A. L. F., Taborda, D. M. G., and Grazina, J. C. D. (2017). Critical State-Based Interpretation of the Monotonic Behavior of Hostun Sand. Journal of Geotechnical and Geoenvironmental Engineering, 143(5), pp. 1–14.

Belotti, R., Jamiolkowski, M., Lo Presti, D. C. F. and O'Neill, D. A. (1996). Anisotropy of small strain stiffness in Ticino sand. Géotechnique, 46(1), pp. 115–131.

Bui, M. T. (2009). Influence of some particle characteristics on the small strain response of granular materials, PhD thesis, University of Southampton.

Chaudhary, S. K., Kuwano, J. and Hayano, Y. (2004). Measurement of quasi-elastic stiffness parameters of dense Toyoura sand in hollow cylinder apparatus and triaxial apparatus with bender elements. Geotechnical Testing Journal, 27(1), pp. 23-35.

Cho, G. C., Dodds, J. and Santamarina, J. C. (2006). Particle shape effects on packing density, stiffness, and strength: natural and crushed sands, Journal of Geotechnical and Geoenvironmental Engineering, 132(5), pp. 591–602.

Fioravante, V. (2000). Anisotropy of small strain stiffness of Ticino and Kenya sands from seismic wave propagation measured in triaxial testing. Soils and Foundations, 40(4), pp. 129-142.

Gasparre, A., Nishimura, S., Minh, N.A., Coop, M.R. and Jardine, R.J. (2007). The stiffness of natural London Clay. Géotechnique, 57(1), pp. 33-47.

Goudarzy, M. (2015). Micro and macro mechanical assessment of small and intermediate strain properties of granular material. PhD thesis, Ruhr-Universität Bochum, Bochum, Germany.

Goudarzy, M., Rahman, M. M., König, D., and Schanz, T. (2016). Influence of non-plastic fines content on maximum shear modulus of granular materials. Soils and Foundations, 56(6), pp 973–983.

Goudarzy, M., König, D., Santamarina, J. C. and Schanz, T. (2018). The influence of the anisotropic stress state on the intermediate strain properties of granular material, Géotechnique, 68(3), pp. 221-232.

Goudarzy, M. and Wichtmann, T. (2019). Influences of particle characteristics on the instability and dynamic characteristics of granular materials. Fachsektionstage Geotechnik Congress Centrum Würzburg, Germany, October 29-30, 2019.

Gu, Q., König, D. and Goudarzy, M. (2020). Influence of the sample preparation on the mechanical characteristics of Hostun sand, Geotechnical Engineering Journal of the SEAGS & AGSSEA, 51 (4), ISSN 0046-5828.

Hardin, B.O. and Richart, E.F.Jr. (1963). Elastic Wave Velocities in Granular Soils. Journal of the Soil Mechanics and Foundation Division, ASCE, 89(1), pp. 33–65.

Hardin, B.O. and Black, W.L. (1966). Sand stiffness under various triaxial stresses. Journal of Soil Mecanics and Foundation Engineering Division (ASCE), 92(2), pp. 27–42.

Hardin, B. O. and Kalinski, M. E. (2005). Estimating the shear modulus of gravelly soils. Journal of Geotechnical and Geoenvironmental Engineering, 131(7), pp. 867-875.

Iwasaki, T. and Tatsuoka, F. (1977). Effects of grain size and grading on dynamic shear moduli of sands. Soils and Foundations, 17(3), pp.19-35.

Jamiolkowski, M., Lancellotta, R. and Lo Presti, D. C. (1995). Remarks on the stiffness at small strains of six Italian clays. In Proceedings of Pre-failure deformation of geomaterials: the international symposium, Japan, AA Balkema, pp. 817-836.

Kuribayashi, E., Iwasaki, T. and Tatsuoka, F. (1975). Effects of stress-strain conditions on dynamic properties of sands. JSCE Proceedings, 242, pp. 105-114.

Kuwano, R. and Jardine, R.J. (2002). On the applicability of cross-anisotropic elasticity to granular materials at very small strains. Géotechnique, 52(10), pp. 727-749.

Lo Presti, D.C.F., Jamiolkowski, M., Pallara, O., Cavallaro, A. and Pedroni, S. (1997). Shear Modulus and Damping of Soils. Géotechnique, 47(3), pp. 603–617.

Menq F. Y. and Stokoe, II K. H. (2003). Linear dynamic properties of sandy and gravelly soils from large-scale resonant tests. In: Di Benedetto H, Doanh T, Geoffroy H, Sauzeat C, editors. Deformation characteristics of geomaterials. Lisse: Swets & Zeitlinger, pp. 63–71.

Payan, M., Khoshghalb, A., Senetakis, K. and Khalili, N. (2016). Small-strain stiffness of sand subjected to stress anisotropy, Soil Dynamics and Earthquake Engineering, 88, pp. 143-151.

Pennington, D.S., Nash, D.F.T. and Lings, M.L. (1997). Anisotropy of G0 shear stiffness in Gault Clay. Géotechnique, 47(3), pp. 391-398.

Roesler, S. (1979). Anisotropic shear modulus due to stress anisotropy. J Geotech Eng Div, 105, pp. 871–880.

Sadek, T., Lings, M., Dihoru, L. and Wood, D. M. (2007). Wave transmission in hostun sand: multiaxial experiments. Rivista Italiana Geotecnica, 41(2), pp. 69–84.

Santamarina, C. and Cascante, G. (1996). Stress anisotropy and wave propagation: a micromechanical view, Can. Geotech. J., 33(5), pp. 770–782.

Sarkar, D., Goudarzy, M. and König, D. (2019). An interpretation of the influence of particle shape on the mechanical behavior of granular material. Granular Matter, 21:53, pp. 1-24.

Senetakis, K., Anastasiadis, A. and Pitilakis, K. (2012). Small strain shear modulus and damping ratio of quartz and volcanic sands, Geotechnical Testing Journal, 35(6), pp. 1-17.

Shi, J., Haegeman, W. and Cnudde, V. (2021). Anisotropic small strain stiffness of calcareous sand affected by sample preparation, particle characteristic and gradation. Géotechnique, 71(4), pp. 305-319.

Wang, Y. H. and Mok, C. M. (2008). Mechanisms of Small-Strain Shear-Modulus Anisotropy in Soils. Journal of Geotechnical and Geoenvironmental Engineering, 134(10), pp. 1516-1530.

Wichtmann, T. and Triantafyllidis, T. (2009). Influence of the grain size distribution curve of quartz sand on the small strain shear modulus G_{max}, Journal of Geotechnical and Geoenvironmental Engineering, 135 (10), pp. 1404-1418.

Yang, J. and Gu, X. Q. (2013). Shear stiffness of granular material at small strains: does it depend on grain size? Géotechnique, 63 (2), pp. 165-179.

Yamashita, S., Hori, T. and Suzuki, T., (2005). Effects of initial and induced anisotropy on initial stiffness of sand by triaxial and bender elements tests. In Geomechanics: Testing, modeling, and simulation (pp. 350-369).

Yamashita. S., Kawaguchi, T., Nakata, Y., Mikami, T., Fujiwara, T., and Shibuya, S. (2009). Interpretation of international parallel test on the measurement of G_{max} using bender elements. Soils and Foundations, 49, Issue 4, pp. 631–650.

Yu, P. & Richart, F. (1984). Stress ratio effects on shear modulus of dry sands. Journal of Geotechnical Engineering, 110(3), pp. 331–345.